THE JOURNAL OF BIOLOGICAL CHEMISTRY VOL. 282, NO. 13, pp. 9713–9721, March 30, 2007

The Structure of Apolipoprotein A-II in Discoidal High Density Lipoproteins*

Received for publication, November 7, 2006, and in revised form, January 25, 2007 Published, JBC Papers in Press, January 30, 2007, DOI 10.1074/jbc.M610380200

R. A. Gangani D. Silva[‡], Lumelle A. Schneeweis[§1], Srinivasan C. Krishnan[¶], Xiuqi Zhang[‖], Paul H. Axelsen[§1], and W. Sean Davidson[‡2]

From the [‡]Department of Pathology and Laboratory Medicine, University of Cincinnati, Cincinnati, Ohio 45237, the [§]Departments of Pharmacology, Biochemistry, and Biophysics, University of Pennsylvania, Philadelphia, Pennsylvania 19104, the [¶]Mass Spectrometry Application Laboratory, Applied Biosystems, Framingham, Massachusetts 01701, and the [‖]Department of Chemistry, University of Illinois, Chicago, Illinois 60607

It is well accepted that high levels of high density lipoproteins (HDL) reduce the risk of atherosclerosis in humans. Apolipoprotein A-I (apoA-I) and apoA-II are the first and second most common protein constituents of HDL. Unlike apoA-I, detailed structural models for apoA-II in HDL are not available. Here, we present a structural model of apoA-II in reconstituted HDL (rHDL) based on two well established experimental approaches: chemical cross-linking/mass spectrometry (MS) and internal reflection infrared spectroscopy. Homogeneous apoA-II rHDL were reacted with a cross-linking agent to link proximal lysine residues. Upon tryptic digestion, cross-linked peptides were identified by electrospray mass spectrometry. 14 cross-links were identified and confirmed by tandem mass spectrometry (MS/MS). Infrared spectroscopy indicated a beltlike molecular arrangement for apoA-II in which the protein helices wrap around the lipid bilayer rHDL disc. The cross-links were then evaluated on three potential belt arrangements. The data clearly refute a parallel model but support two antiparallel models, especially a "double hairpin" form. These models form the basis for understanding apoA-II structure in more complex HDL particles.

High density lipoproteins (HDL)[3] have received a great deal of attention in recent years due to postulated roles in atheroprotective processes, such as reverse cholesterol transport, anti-inflammation, and anti-oxidation. Apolipoprotein A-I (apoA-I) is the most abundant protein in HDL (at about 1 mg/ml in plasma) and clearly modulates many HDL atheroprotective functions. By contrast, there is much less known about the second most abundant protein, apoA-II. The average apoA-I/apoA-II molecular ratio in human plasma is 2:1, hinting that such an abundant protein should have important physiological functions. Murine studies with either human or mouse transgenes showed that apoA-II overexpression creates a more atherogenic lipoprotein profile (1–4). On the other hand, apoA-II knock-out mice exhibited dramatically decreased HDL cholesterol levels (5). However, these studies have not provided a clearly recognized function for apoA-II.

There is evidence that a small amount of HDL in human plasma contains apoA-II as its only protein constituent (6). Moreover, this apoA-II-only HDL (LpA-II-HDL) dominates in patients with Tangier disease, presumably compensating for the lack of apoA-I in HDL (6). Recently, it was suggested that nascent LpA-II-HDL and LpA-I-HDL may fuse to form mature HDL particles in plasma (7, 8). However, most circulating apoA-II is present in LpA-I/A-II mixed HDL particles. There is growing evidence that one role of apoA-II may be to modulate apoA-I structure, potentially modulating HDL function. Structural studies on LpA-I/A-II particles suggest that apoA-II can cause profound conformational changes in apoA-I (9, 10). One functional study compared the hydrolysis rates of LpA-I, LpA-II, and LpA-I/A-II HDL by endothelial lipase, an important enzyme in physiological regulation of HDL levels (11). The lipid hydrolysis rate was found to be highest in the mixed particles but lower in LpA-I reconstituted HDL (rHDL) and almost undetectable in LpA-II particles. The fact that apoA-II facilitates hydrolysis of lipids in mixed particles but not in A-II rHDL suggests that apoA-II can affect apoA-I conformation to stimulate endothelial lipase activation. Unfortunately, little information exists on the structural interactions between apoA-I and apoA-II, and understanding of apoA-II structure has not kept pace with recent advancements for apoA-I (12).

In human plasma, almost all apoA-II exists as a homodimer, consisting of a single S-S bridge formed across the Cys residue at position 6 of each polypeptide (13). Monomeric apoA-II is 77 residues long with three assigned putative amphipathic helices. ApoA-II was recently crystallized with the lipid surrogate, β-octyl glucoside (BOG) (14). The resulting structure indicated that the apoA-II·BOG complex was composed of eight apoA-II homodimers winding around themselves in a circular spiral-like arrangement in a head-to-tail manner.

* This work was supported in part by NHLBI, National Institutes of Health (NIH), Grant RO1-HL67093 (to W. S. D.) and an American Heart Association Ohio Valley Affiliate postdoctoral fellowship (to R. A. G. D. S.). The costs of publication of this article were defrayed in part by the payment of page charges. This article must therefore be hereby marked "*advertisement*" in accordance with 18 U.S.C. Section 1734 solely to indicate this fact.

[1] Supported by NIH Grant RO1-HL68186.

[2] To whom correspondence should be addressed: Dept. of Pathology and Laboratory Medicine, University of Cincinnati, 2120 Galbraith Rd., Cincinnati, OH 45237-0507. Tel.: 513-558-3707; Fax: 513-558-1312; E-mail: Sean.Davidson@UC.edu.

[3] The abbreviations used are: HDL, high density lipoprotein(s); apo, apolipoprotein; BOG, β-octyl glucoside; BS[3], bis(sulfosuccinimidyl)suberate; DMPC, 1,2-dimyristoyl-*sn*-glycero-3-phosphocholine; HPLC, high performance liquid chromatography; MS, mass spectrometry; MS/MS, tandem mass spectrometry; PATIR-FTIR, polarized attenuated total internal reflection Fourier transform infrared; POPC, 1-palmitoyl-2-oleoyl-*sn*-glycero-3-phosphatidylcholine; PS, anionic lipid variants of DMPC or POPC; rHDL, reconstituted HDL.

However, the relationship of this structure to physiological lipid-containing particles is not clear. ApoA-II-containing rHDL particles containing 1,2-dimyristoyl-*sn*-glycero-3-phosphocholine (DMPC) have been subjected to limited proteolysis analyses (15). The data indicate that lipid-bound apoA-II is more resistant to proteolysis than the lipid-free form and has an entirely different cleavage pattern, indicating significant conformational changes. However, the conformational details of apoA-II structure in native-like HDL particles are not known.

In this study, we used two independent and powerful approaches to gain structural information on apoA-II in native-like HDL particles. The results indicate that apoA-II adopts a "belt-like" orientation similar to that proposed for apoA-I and apoE (16, 17). We propose one of the first detailed models for the three-dimensional arrangement of apoA-II in rHDL particles.

EXPERIMENTAL PROCEDURES

ApoA-II Purification and Preparation of rHDL Particles—Human apoA-II isolation and purification from normolipidemic subjects was carried out as reported previously for apoA-I (9, 18). In brief, after HDL isolation by ultracentrifugation and delipidation, fractions corresponding to apoA-II and apoA-I were collected from a Q-Sepharose fast flow anionic exchange column. The isolated proteins were then passed over a Superdex 200 gel filtration column (Amersham Biosciences) prior to the particle reconstitution reaction. The Bio-bead/cholate removal method was used for the preparation of rHDL particles of apoA-II, as has been reported for apoA-I (19–21). The dimeric (*i.e.* physiological) form of apoA-II was used. Phospholipid, 1-palmitoyl-2-oleoyl-*sn*-glycero-3 phosphatidylcholine (POPC; Avanti Polar Lipids, Birmingham, AL) was used as the sole lipid component in particle reconstitution (Table 1). Particles that are designated as A-I-POPC-rHDL and A-II-POPC-rHDL were reconstituted with starting molar ratios of 1:78 apoA-I/POPC and 1:58 apoA-II/POPC, respectively (Table 1). The rHDL particles that were subjected to infrared spectroscopic analysis were prepared, incorporating the anionic analog of POPC, 1-palmitoyl-2-oleoyl-*sn*-glycero-3-(phospho-L-serine), in a 1:9 molar ratio with POPC as required by the technique (Table 1). These particles, which contain 10 mol % of anionic lipids are designated as A-I-POPC/PS-rHDL and A-II-POPC/PS-rHDL and were prepared with 1:78 and 1:58 starting protein to total lipid ratios (Table 1). Once prepared, the rHDL was repurified using a tandem gel filtration column setup (Superdex 200 and Superose 6; Amersham Biosciences) equilibrated in phosphate-buffered saline (pH 7.8) to remove any unreacted lipids and proteins.

Determination of Number of Protein Molecules per rHDL Particle—The cross-linker 1-ethyl-3-[3-dimethylaminopropyl] carbodimide hydrochloride dissolved in water at 10 mg/ml (Pierce) was added to A-I-POPC-rHDL and A-II-POPC-rHDL in phosphate-buffered saline at a 1 mg/ml protein concentration. The protein/cross-linker molar ratios used were either 1:50 or 1:500. The sample solutions were incubated at 4 °C for 24 h and then subjected to PAGE analysis.

Cross-linking and Tryptic Digestion of ApoA-II—Freshly prepared bis(sulfosuccinimidyl) suberate (BS^3) cross-linker (6.5 mg/ml in phosphate-buffered saline, pH 7.8) (Pierce) was added to homogeneous A-II-POPC-rHDL with 1 mg/ml protein concentration, at a protein/BS^3 molar ratio of 1:10. The BS^3 solution preparation and the addition to the protein were performed within 1 min to minimize hydrolysis of the cross-linker, as was described previously (20, 22). Samples were incubated at 4 °C for 24 h. The samples were lipid-extracted using standard chloroform/methanol extraction procedures. The cross-linked protein was resolubilized in 3 M guanidine in 5 mM ammonium bicarbonate, dialyzed into 5 mM ammonium bicarbonate, and concentrated by ultrafiltration (YM-10; Millipore Corp., Bradford, MA). The protein samples were digested using 2.5% (w/w) sequencing grade trypsin (Promega) and incubating at 37 °C for ~12 h, followed by a second aliquot of trypsin at the same ratio for an additional 2 h. The samples (50 μg protein aliquots) were lyophilized and stored at −20 °C until used in the mass spectrometry analysis.

Tryptic Peptide Analysis by Nanoliquid Chromatography and Mass Spectrometry—Peptide mass detection was carried out on an Applied Biosystems MDS Sciex QStar® XL mass spectrometer equipped with a nanospray ion source following separation of the peptides on nanoflow high performance liquid chromatography (HPLC) from LC Packings. Five pmol of the peptides generated from trypsin digestion of the cross-linked apoA-II were injected onto a C18 Trap cartridge (from LC Packings; 300-μm inner diameter and 1-mm length) and washed with 0.1% trifluoroacetic acid, 0.1% formic acid in water flowing at 20 μl/min for 20 min. This was followed by elution of the peptides onto a C18 nanoanalytical column (75-μm inner diameter and 15-cm length from LC Packings) for separation using a gradient of acetonitrile from 5 to 40% at a flow rate of 250 nl/min over 90 min. The gradient was generated using solvent A (0.1% formic acid, 0.01% trifluoroacetic acid, 2% acetonitrile in HPLC grade water) and solvent B (0.1% formic acid, 0.01% trifluoroacetic acid, 2% water, 10% isopropyl alcohol in acetonitrile). Under these conditions, most peptide masses were well separated as seen by the total ion chromatogram. The mass spectrometer was set to acquire MS and MS/MS data in an automated fashion using the information-dependent acquisition functionality of the Analyst® QS software. Each MS spectrum acquired in 1 s was followed by acquisition of four MS/MS spectra at 3 s each of the four most intense ions after satisfying the dynamic exclusion criteria. The dynamic exclusion criteria allowed for generating an exclusion list of peptide masses already fragmented for a period of 60 s with a mass tolerance of 100 ppm for match of peptide mass. Upon completion of the liquid chromatography/MS/MS run, a peptide mass list was generated using the Applied Biosystems Analyst QS 1.1 software. The mass list was subjected to analysis by GPMAW (ChemSW, Inc.) to assign putative sequence identity of individual peptides with or without a modification by a cross-linker (19, 20, 22). The putative amino acid sequence identity of the interpeptide cross-linked masses were assigned by mass mapping of experimental masses with a theoretically constructed list of all possible intra-/intermolecularly cross-linked masses for apoA-II (19, 20, 22). A map was considered positive if the experimental and theoretical

masses came within 10 ppm with the correct number of Lys residues available for the cross-linker formation (19). This deviation is a considerable improvement compared with our previous cut-off of 50 ppm (19, 20, 22), a result of hardware and technique improvements. Confirmation of peptide identities was provided by MS/MS analysis.

Particle Characterization by CD Spectroscopy—CD spectra of rHDL particles that contained POPC only, POPC/PS, and free proteins (apoA-II and apoA-I) in 5 mM standard Tris buffer were measured on a J-810 spectrometer (Jasco, Easton, MD). A homemade demountable cell composed of two UV CaF_2 windows separated by a 100-μm Teflon spacer clamped in a brass holder was used in the sample measurements. Such a set up for the cell was required due to the use of a relatively high protein concentration of 0.225 mg/ml. A scan rate of 20 nm/min and a bandwidth of 0.2 nm with a time response of 2 s were used to obtain CD spectra as an average of eight scans. The final spectra were obtained by subtracting a background spectrum of the same buffer. The fractional secondary structure of the proteins in solution was estimated from the CD spectra by use of the SELCON 3 method, which is part of the CD-Pro software package (23).

Fluorescence Studies—Fluorescence measurements of POPC, POPC/PS rHDL particles, and free proteins (apoA-II and apoA-I) were performed on a Fluoromax-3 spectrofluorometer (Jobin Yvon Inc., Edison, NJ) on 0.225-mg/ml samples in a 1-mm quartz cuvette. The excitation wavelengths were 275 nm (Tyr excitation for apoA-II) and 295 nm (Trp excitation for apoA-I). The emission spectra for both were recorded from 300 to 450 nm. In all experiments, a background spectrum of the buffer was subtracted from the corresponding sample spectra.

Infrared Spectroscopy—Polarized attenuated total internal reflection Fourier transform infrared (PATIR-FTIR) spectroscopy was performed on A-II-POPC/PS-rHDL and A-I-POPC/PS-rHDL. We included an rHDL particle as a positive control that had been analyzed previously (16). The control particle contained apoA-I with DMPC/1,2-dimyristoyl-*sn*-glycero-3-(phosphor-L-serine). The protein/total lipid ratio for these particles (A-II-DMPC/PS-rHDL) was 1:78 with 10% 1,2-dimyristoyl-*sn*-glycero-3-(phosphor-L-serine) in the lipid mixture as for other particles that were subjected to PATIR-FTIR analysis. The PATIR-FTIR measurements were carried out using a Bio-Rad FTS-6000 spectrometer equipped with an MCT detector. The instrument was interfaced to a lipid film balance by means of a horizontal 50 × 10 × 2-mm germanium crystal internal reflection element. A lipid monolayer composed of 80 mol % DMPC and 20 mol % 1,2-dimyristoyl-*sn*-glycero-3-(phosphor-L-serine) was spread at room temperature at the air-water interface in the film balance and applied flat onto the crystal. Adsorption of the HDL particles and their horizontal orientation was facilitated by Ca^{2+} ions in the buffer bridging the anionic lipid in the monolayer (20 mol %) and in the complexes (10 mol %) (16). All spectra were collected in the rapid scan mode as 512 co-added interferograms, with a resolution of 2 cm^{-1}, scanning speed of 20 MHz, triangular apodization, and one level of zero filling. Base-line spectra were recorded immediately prior to the addition of 20 μg of protein in the form of lipoprotein complexes to the continuously stirred buffer subphase composed of 30 mM HEPES, 1 mM $CaCl_2$, in D_2O at pD 7.4.

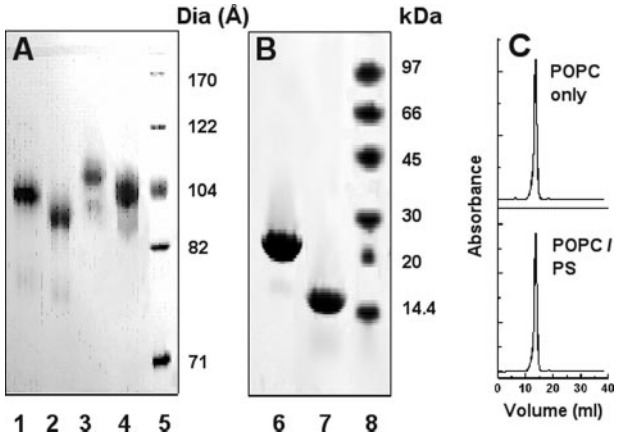

FIGURE 1. **PAGE analysis of A-I-rHDL and A-II-rHDL particles.** rHDL particles were generated either with POPC only or with a 9:1 mixture of POPC/PS as required for different experiments. *A*, native PAGE analysis (8–25% Phast gel) showing the apparent hydrodynamic diameters of A-I-POPC-rHDL (*lane 1*), A-I-POPC/PS-rHDL (*lane 2*), apoA-II-POPC-rHDL (*lane 3*), and apoA-II-POPC/PS-rHDL (*lane 4*). *B*, SDS-PAGE analysis (8–25% Phast gel) showing apoA-I (*lane 6*) and apoA-II (*lane 7*) in POPC-rHDL particles prior to cross-linking. High molecular weight markers are shown in *lanes 5* (GE Healthcare, Amersham Biosciences high molecular weight standards; catalog number 17-0445-01). Hydrodynamic diameters corresponding to the high molecular weight standards were taken from the literature (31). The low molecular weight standards are shown in *lane 8* (GE Healthcare, Amersham Biosciences low molecular weight standards; catalog number 17-0446-01). Both gels were stained with Coomassie Blue. *C*, fast protein liquid chromatography traces of A-I-POPC-rHDL (*top*) and A-I-POPC/PS-rHDL (*bottom*).

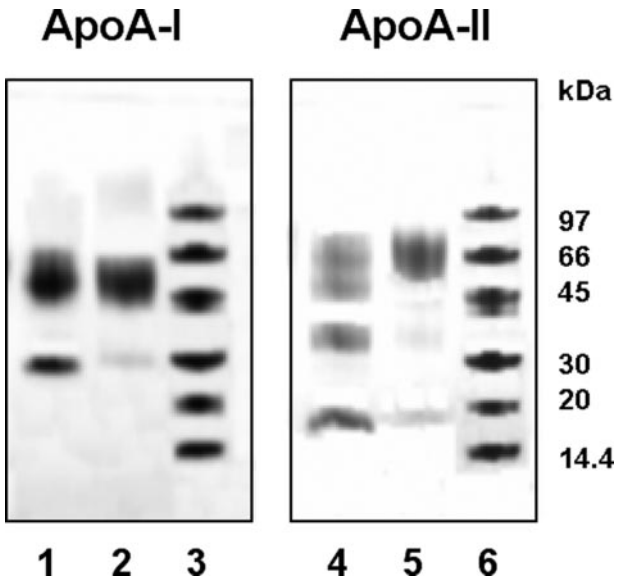

FIGURE 2. **SDS-PAGE analysis of cross-linked A-I-POPC-rHDL and A-II-POPC-rHDL particles.** The number of protein molecules per rHDL particle was determined by cross-linking the particles with 1-ethyl-3-[3-dimethylaminopropyl]carbodiimide hydrochloride in a 1:50 protein/cross-linker ratio (*lanes 1* and *4*) and at a 1:500 ratio (*lanes 2* and *5*). Low molecular weight standards (see Fig. 1) are shown in *lanes 3* and *6*. The gels were stained with Coomassie Blue.

From the polarized absorption spectra, dichroic ratios were evaluated using integrated areas of characteristic absorption bands as determined by linked analysis of sets of parallel and perpendicular spectra. These dichroic ratios were then converted to order parameters $S(R_z)$ as described

TABLE 1
Compositional analysis of rHDL particles

rHDL[a]	Protein/PL (start)	Protein/PL (final)[b]	Hydrodynamic diameter (Å)[c]	Protein molecules/particle[d]
A-I-POPC-rHDL	1:78	1:78 ± 4	96 ± 1	2
A-I-POPC/PS-rHDL	1:78	1:84 ± 4	ND[e]	2
A-II-POPC-rHDL	1:58	1:48 ± 2	102 ± 1	4
A-II-POPC/PS-rHDL	1:58	1:51 ± 2	ND	4

[a] In cases where both lipids were used, the POPC/PS molar ratio is 9:1.
[b] Final protein/phospholipid (PL) ratios are based on Lowry and the phosphorus assays on purified rHDL particles (33).
[c] Average apparent particle diameters were calculated based on migration distance on a native gel (PAGE) using three independent particle preparations. Particles that contain anionic lipids (PS) were not subjected to hydrodynamic diameter calculations using this method because of charge effects due to the presence of the anionic lipid (see "Results").
[d] Number of protein molecules per rHDL particle is obtained by cross-linking followed by SDS-PAGE analysis (Fig. 2).
[e] ND, not determined.

(16, 24). An order parameter of $S = 1.0$ indicates a uniform orientation perpendicular to the membrane surface, whereas a value of $S = -0.5$ indicates a uniform orientation parallel to the membrane. An order parameter of $S = 0.0$ may indicate an isotropic distribution, a uniform orientation at the magic angle ($\theta = 54.7°$ relative to the membrane normal), or any distribution for which $\langle \cos^2 \theta \rangle = \frac{1}{3}$.

RESULTS

Generation and Characterization of A-II-POPC-rHDL Particles—We hypothesized that apoA-II, like apoA-I, adopts a specific conformation in discoidal rHDL and therefore exhibits sequence-specific interactions with itself and with other apoA-II molecules on the particle (19, 20, 25). We elected to generate apoA-II-containing rHDL particles that contain POPC, a synthetic lipid with an acyl chain composition commonly found in cellular membranes and lipoproteins. At a starting ratio of 58 mol of POPC to 1 mol of apoA-II, we were able to reconstitute A-II-POPC-rHDL that exhibited a slightly larger hydrodynamic diameter than previously well characterized A-I-POPC-rHDL (Fig. 1*A*) (20, 26, 27). Despite our best efforts, we were unable to eliminate a minor secondary band, which ran a few Å smaller than the major band at ~102 Å. The number of protein molecules per particle was determined by cross-linking with 1-ethyl-3-[3-dimethylaminopropyl]carbodiimide hydrochloride, which can bridge an acidic amino acid (Asp or Glu) with a Lys residue (28, 29). When cross-linked at a high ratio of protein to 1-ethyl-3-[3-dimethylaminopropyl]carbodiimide hydrochloride, the A-II-POPC-rHDL sample exhibited a single band of ~70 kDa corresponding to the mass of four dimeric apoA-II molecules (Fig. 2). At lower cross-linker ratios, bands corresponding to 1, 2, 3, and 4 molecules of apoA-II[4] were apparent, indicating incomplete cross-linking. No other condition yielded molecular weight bands higher than four cross-linked molecules of apoA-II. A similar analysis for an A-I-POPC-rHDL particle yielded the expected 2 molecules of apoA-I per particle (Fig. 2). Component analysis on the rHDL (after isolation from unreacted protein and lipid) indicated that the A-II-POPC-rHDL contained ~190 POPC molecules/particle compared with ~156 POPC molecules for A-I-POPC-rHDL (Table 1). The increased lipid in the apoA-II particle probably accounts for its larger apparent diameter (Fig. 1*A*).

[4] Human apoA-II is most commonly found in circulation as a disulfide-linked homodimer of 77-amino acid apoA-II polypeptides. For the purposes of this work, we use the term "molecule" to refer to this apoA-II homodimer. We refer to each polypeptide constituent of this molecule as a "strand."

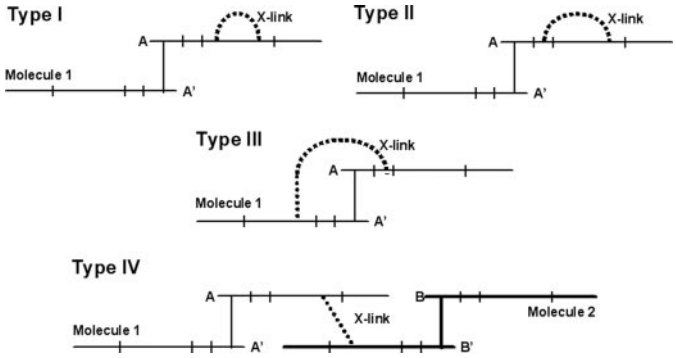

FIGURE 3. **Types of potential cross-links within and between molecules of apoA-II on a discoidal particle.** Two apoA-II molecules are shown as *thick* and *thin solid lines*, with each strand labeled (*A* and *A′* in molecule 1 and *B* and *B′* in molecule 2). Hypothetical tryptic cleavage sites are shown as *short vertical line segments* across the strands. Type I, an intrapeptide cross-link, can occur between two Lys residues on the same tryptic peptide within a single strand of apoA-II. Type II, an interpeptide, intrastrand cross-link, forms within the same strand of apoA-II but across at least one tryptic cleavage site. Type III, an interstrand, intramolecular cross-link, forms between two apoA-II strands that are already joined by the disulfide linkage. Type IV, an interstrand, intermolecular cross-link, forms between two strands of two different apoA-II molecules. These are the only cross-links capable of producing the oligomeric species observed in Fig. 2.

Cross-linking and Mass Spectrometry Analyses—Cross-linking experiments for structural analyses were performed with BS^3, a homobifunctional cross-linker capable of linking Lys residues within its spacer arm length of 11.4 Å. A molar ratio of 1:10 protein/cross-linker was used based on previous work demonstrating that linkages formed under these conditions occur within a single rHDL particle but not between two rHDL particles (19, 20). After cross-linking, the particles were delipidated, digested with trypsin, and analyzed by electrospray MS. In theory, there can be four types of cross-links for apoA-II, as illustrated in Fig. 3. Type I intrapeptide cross-links occur between two Lys residues within the same tryptic peptide. Type II joins two peptides from the same apoA-II monomer but separated by at least one tryptic cleavage site. Type III joins two peptides within the same dimeric apoA-II molecule but on different strands. Type IV joins two peptides from different apoA-II molecules. We identified five Type I intrapeptide cross-links (Table 2). The same set of Type I cross-links was identified from two independent particle preparations. We also identified nine long range, interpeptide cross-links (Table 3). These consisted of two peptides separated by at least a single tryptic cleavage site. Due to the small size of apoA-II, we were unable to assign most of these cross-links to the scheme illustrated in Fig. 3 (*i.e.* they can be Types II, III, or IV). The excep-

TABLE 2
Intrapeptide (Type I) cross-links identified in an apoA-II rHDL particle cross-linked with BS^3

Peptide involved	X-link (Lys-Lys)	Experimental mass	Theoretical mass	Deviation
		Da	*Da*	*±ppm*
24–39	28–30	1953.0124	1953.0126	0
29–44	30–39	1991.0249	1991.0154	5
31–46	39–44	1978.9928	1978.9885	2
40–54	44–46	1948.0411	1948.0554	7
45–55	46–54	1421.8399	1421.8491	6

TABLE 3
Interpeptide cross-links (Type II, III, or IV) identified in an apoA-II rHDL particle X-linked with BS^3

Peptides involved	X-link (Lys-Lys)	Experimental mass	Theoretical mass	Deviation
		Da	*Da*	*±ppm*
24–30, 40–46	28–44	1886.9568	1886.9697	6.8
29–39, 40–46	30–44	2224.1532	2224.1625	4.2
29–39, 45–54	30–46[a]	2492.4152	2492.4099	2.1
29–39, 47–55	30–54	2405.3712	2405.3779	3.2
31–44, 45–54	39–46	2919.5358	2919.5478	4.1
31–44, 47–55	39–54	2832.5163	2832.5158	0.2
40–46, 47–55	44–54	2094.1470	2094.1610	6.6
40–46, 55–77	44–55	3537.8244	3537.7920	9.1
45–54, 45–54	46–46	2449.4373	2449.4404	1.2

[a] All cross-links were identified in both experiments carried out on two independent sample preparations. The cross-link 30–46 was identified in one experiment.

tion is the cross-link Lys^{46}-Lys^{46}, which must be either Type III or IV but not II. MS/MS sequencing of these long range cross-links indicated that each putative sequence had more than 50% of the expected theoretical fragment ions, unambiguously confirming the sequences of the assigned peptides. An example analysis is shown in Fig. 4. Interestingly, we found no evidence for either Lys^3 or Lys^{23} modification by BS^3. However, unmodified peptides in this region were clearly identified in the spectra (*e.g.* two copies of peptide 4–23 linked by an S–S bond found at m/z 1146.5349 (charge state +4), corresponding to molecular weight 4582.1084.

Molecular Orientation of ApoA-II on Discoidal rHDL Particles—In order to use the cross-link distance constraints listed in Tables 2 and 3 to propose models for apoA-II structure on the edge of discoidal rHDL, it was necessary to determine the orientation of the apoA-II backbone. Based on previous success with apoA-I and apoE rHDL, PATIR-FTIR spectroscopy was chosen for this purpose (16, 17). As noted under "Experimental Procedures," this technique requires the incorporation of a small amount of anionic lipid into the particles in order to sequester and align them during the measurements. Table 1 shows that the anionic lipid (1-palmitoyl-2-oleoyl-*sn*-glycero-3-(phospho-L-serine))-containing particles (POPC/PS) exhibited a composition similar to that of the particles that contain only POPC. When analyzed by native PAGE (Fig. 1), the POPC/PS particles appeared to migrate faster than the POPC particles with an apparent diameter of ~100 nm. However, gel filtration chromatography indicated that the POPC/PS particles exhibited the exact same retention volume as the POPC particles, indicating that the two particles were of similar hydrodynamic diameter. The example of the apoA-I-containing particles is shown in Fig. 1*C*. It is likely that the faster migration of POPC/PS particles on the native gel was due to the increased negative charge imparted by the added anionic lipid. ApoA-II particles prepared with and without anionic lipids (A-II-POPC/PS-rHDL and A-II-POPC-rHDL) exhibited similar circular dichroism spectral signatures (Fig. 5*A*), indicating similar overall secondary structural contents. Analysis of the spectra indicated that A-II-POPC-rHDL and A-II-POPC/PS-rHDL had 79 ± 5 and 75 ± 5% α-helical contents, respectively. Fluorescence emission spectra of A-II-POPC/PS-rHDL and A-II-POPC-rHDL particles were also similar (Fig. 5*B*). Based on these data, we concluded that PS inclusion minimally affected particle structure. Similar CD and fluorescence analyses carried out on apoA-I particles indicated that A-I-POPC/PS-rHDL and A-I-POPC-rHDL were similar in structure as well (data not shown).

PATIR-FTIR spectroscopy was performed on three different rHDL particles: A-II-POPC/PS-rHDL, A-I-POPC/PS-rHDL, and A-I-DMPC/PS-rHDL. The particles studied as a control, A-I-DMPC/PS-rHDL, were homogeneous, as seen by native PAGE, and contained ~216 lipid molecules/particle (data not shown). These were studied to assure that modifications to the instrumentation made since these particles were last examined did not change the results (Table 4) (16). Second, we examined A-I-POPC/PS-rHDL particles to determine the effect of longer lipid acyl chains on the results. Although there was a trend toward less order and greater variability with longer chain lipids, the orientational relationship between protein and lipid components was unchanged (Table 4). Third, we examined A-II-POPC/PS-rHDL particles. Amide I and methylene stretching bands from A-I-POPC/PS-rHDL and A-II-POPC/PS-rHDL particles are compared in Fig. 6. In both particles, the amide I absorption maximum was located at 1643 cm^{-1}, and both spectra could be fitted with similar components. Likewise, antisymmetric and symmetric methylene stretching bands at ~2924 and ~2854 cm^{-1} from both particles were similar. Most importantly, there was no difference in protein and lipid order parameters (Table 4).

DISCUSSION

This study produced two principal findings. The first was a set of peptide cross-links between specific Lys residues in the native structure of well defined apoA-II rHDL particles. Second, infrared spectroscopy on similar particles indicated that apoA-II adopts a beltlike orientation in which apoA-II wraps around a lipid bilayer parallel to the particle surface. These data, combined with the geometric constraints inherent to the particle phospholipid bilayer, provide sufficient information to propose and test a series of structural models for the apoA-II particles. The results of the infrared spectroscopy measurements are discussed first, followed by an analysis of potential structural models using the cross-links.

The order parameter data in Table 4 show that apoA-II adopts a belt molecular arrangement that is quite similar to that adopted by apoA-I. Thus, apoA-I (16), apoE (17), and apoA-II all adopt a similar general orientation with respect to the lipid bilayer. The results obtained for apoE differed from apoA-I, suggesting that certain apoE regions may associate in the plane of the membrane, possibly perturbing the lipid packing characteristics of the particle. These conclusions were based on an observed decrease in the magnitude of the order parameters for

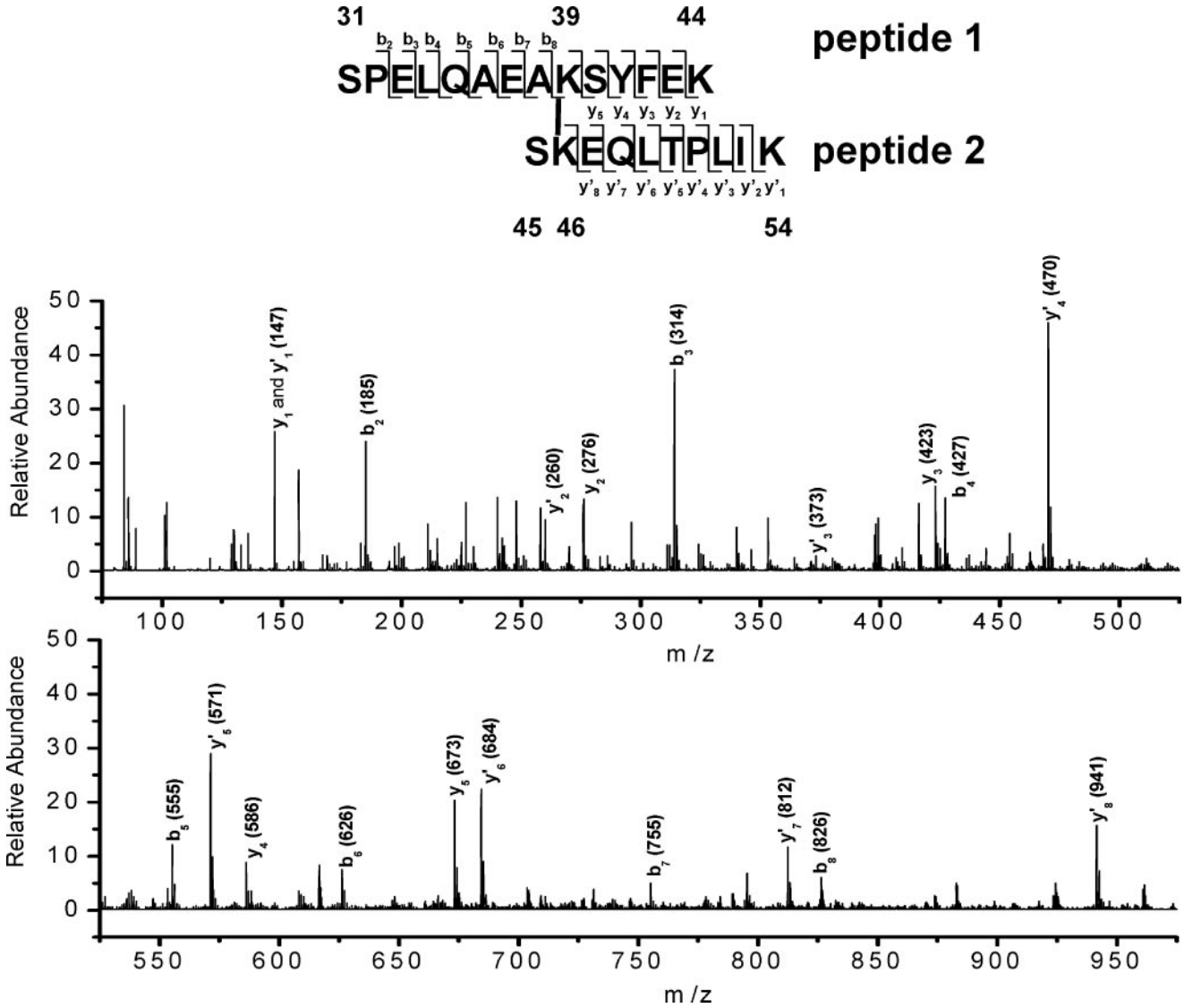

FIGURE 4. **MS/MS sequencing evidence for the cross-link Lys^{39}–Lys^{46}.** Typical MS/MS fragment ions b and y, resulting from different amide bond fragmentations of the precursor ion (m/z = 974.1807, charge state = +3) corresponding to the cross-linked peptide Lys^{39}–Lys^{46} (molecular weight 2919.5478). Note that 20 of 22 expected b and y fragment ions are clearly available in the spectrum. The m/z value that corresponds to charge state +1 is shown *beside* each observed fragment ion. Deaminated forms of the fragments ions (*e.g.* b-NH_3 and y-NH_3) are also present but, for clarity, are not labeled. The *two panels* represent high and low m/z ranges of the same spectrum.

the lipid acyl chains (from −0.45 for Δ(1–43)apoA-I-DMPC/PS to −0.35 apoE-DMPC/PS). In this study, we used the more physiological lipid POPC. The reduced lipid order parameter compared with DMPC-rHDL was most likely due to the introduction of unsaturated acyl chains. This is illustrated by comparing the lipid order parameters for the apoA-I particles with each of these lipids in Table 4. An acyl chain tilt of about 26° for POPC with respect to DMPC could also account for an order parameter near 0.33, but this degree of tilt in such a small particle seems unlikely on geometric grounds. In any case, the lipid order parameter for the A-II-POPC-rHDL particles was comparable with the A-I-POPC-rHDL particles. Thus, unlike apoE, apoA-I and apoA-II do not seem to perturb lipid packing and have overall similar backbone orientations.

A Model for ApoA-II rHDL—Based on theoretical considerations from studies of apoA-I rHDL disc studies, we approached the modeling of apoA-II with the following basic assumptions: 1) the particles are composed of a patch of phospholipid bilayer, and apoA-II is limited to the bilayer edge; 2) the bilayer edge is covered by two continuous or discontinuous amphipathic helical strands of apoA-II (disulfide-linked) with the hydrophobic faces of the amphipathic helices facing the lipids; 3) all four molecules of apoA-II on the particle adopt identical conformations; and 4) the protein backbone is oriented predominantly parallel to the plane of the bilayer. Given these assumptions, we envisioned three general models for apoA-II conformation in the particles (Fig. 7). In the parallel model, all four molecules are oriented in the same direction, making head-to-tail (or in an alternate version, head-to-head) contacts. Fig. 7 shows only two apoA-II molecules for clarity, but additional molecules can be added to the ends with no impact on the cross-linking parameters. In the antiparallel model, the monomeric constituents of each apoA-II molecule are rotated 180° with respect to the disulfide linkage and pro-

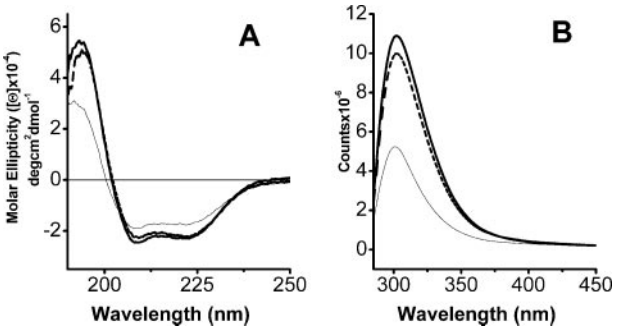

FIGURE 5. **Circular dichroism and fluorescence spectra of A-II-rHDL particles in solution.** *A*, CD spectra of A-II-POPC-rHDL (*thick solid lines*), A-II-POPC/PS-rHDL (*dotted lines*), and free apoA-II (*thin solid lines*) recorded in standard Tris buffer. The spectra were recorded in a 100-μm demountable cell with 0.225 mg/ml sample concentration. *B*, fluorescence spectra of A-II-POPC-rHDL (*thick solid line*), A-II-POPC/PS-rHDL (*dotted line*), and free apoA-II (*thin solid line*) recorded with the same sample concentrations as were CD spectra in a 1-mm quartz cuvette. The fluorescence excitation wavelength was 275 nm, which corresponds to the Tyr absorbance. In both CD and fluorescence measurements, the buffer spectra were subtracted from the corresponding sample spectra.

TABLE 4

Order parameters derived for apoA-II and apoA-I rHDL particles

rHDL complex[a]	Amide I (overall)	Symmetric CH_2 stretch	*n* (number of experiments)
A-I-DMPC/PS-rHDL	−0.16 ± 0.01	−0.42 ± 0.02	3
A-I-POPC/PS-rHDL	−0.14 ± 0.07	−0.34 ± 0.08	3
A-II-POPC/PS-rHDL	−0.13 ± 0.07	−0.33 ± 0.05	4
A-I-DMPC/PS-rHDL(h)[b]	−0.19 ± 0.04	−0.43 ± 0.05	

[a] Component bands centered at 1671, 1645, and 1627 cm^{-1} were integrated and summed to determine order parameters for apoA-I amide I absorption. Components centered at 1652, 1630, and 1617 cm^{-1} were used for the apoA-II amide I absorption. The methylene stretching region from 3000 to 2800 cm^{-1} was fitted with four bands, but only the symmetric CH_2 stretch component at 2854 cm^{-1} was used for order parameter calculations.

[b] The order parameters for A-I-DMPC/PS-rHDL(h) heterogeneous particles reported previously (32).

ceed in opposite directions. Note the extensive intermolecular contacts in this model. An additional antiparallel model exhibits the same rotation about the disulfide linkage but postulates that each apoA-II strand doubles back on itself. We call this the double hairpin model.

We tested these models with the distance constraints derived from the cross-linking data in Tables 2 and 3. We began with the P-Q dimer of apoA-II as determined from the crystal structure in association with the detergent BOG (Fig. 7, *top*) (14). Although not derived from true phospholipid-bound apoA-II, Kumar *et al.* (14) proposed that this pair may be suggestive of a lipid-bound form of apoA-II. In this structure, two monomeric constituents of each apoA-II molecule, lying parallel to each other, wrap around other apoA-II molecules with intermittent detergent molecules bound at an orientation normal to that of the helical segments. The degree of curvature of the P-Q dimer, being at the outer edge of the structure, is relatively consistent with the curvature of a 96-Å apoA-I/phospholipid disc. To generate the antiparallel and double hairpin models, the parallel P-Q dimer structure was graphically manipulated, and a relative distance measuring system was established based on measurements made in the P-Q dimer structure. The 14 intra- and interpeptide cross-links were then tested within each model. In many cases, we were unable to determine if a particular interpeptide cross-link was formed within the same apoA-II strand

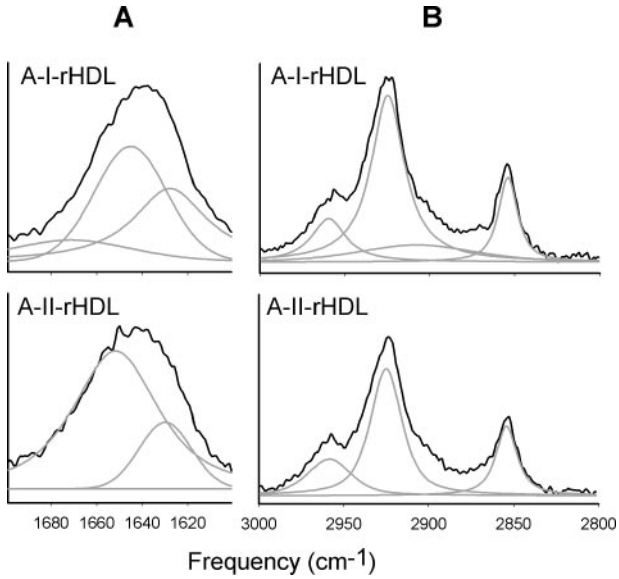

FIGURE 6. **Infrared spectra of A-I- and A-II-POPC/PS-rHDL particles in the lipid methylene stretching and amide I regions.** *A*, both apoA-I and apoA-II rHDL amide I bands are located at ~1643 cm^{-1}. *B*, the antisymmetric and symmetric vibrational bands of the methylene groups of the lipids are located at 2924 and 2854 cm^{-1}, respectively. Fitted component bands are shown as *thin lines* in each spectrum. The dichroic ratios were then used to calculate the order parameters (see "Experimental Procedures") summarized in Table 4.

(*i.e.* Type II) (Fig. 3) or was formed between two separate strands (*i.e.* Type III or IV). Therefore, each cross-link was evaluated for both possibilities. Given the length of two Lys side chains and the cross-linker spacer arm, we previously established that the β-carbons of two Lys residues must reside within about 20 Å in order to form a BS^3 cross-link (20). Therefore, distances of <20 Å for a given cross-link were considered possible for each model, whereas larger distances were considered not possible. The results of this analysis are shown in Table 5. For the parallel model, only 9 of 14 cross-links could fit the data. Many of these included short range cross-links that equally fit all three models. The fits were much more plausible for the antiparallel model, with only two cross-links that were inconsistent with the data. The best fit came for the double hairpin model, with all but one cross-link judged to be plausible. In addition, the distances for most of the cross-links were substantially shorter for this model than for the antiparallel version.

As stated above, the crystal structures of both lipid-free and detergent-bound apoA-II clearly indicate that apoA-II can adopt the parallel model, a least under crystallization conditions. But our analysis shows that five experimentally derived cross-links are simply not consistent with this model in true lipid-bound apoA-II particles in solution. There are also several other compelling arguments against the parallel model. First, our pilot experiments indicated that even low protein to cross-linker ratios are quite capable of linking all four apoA-II molecules in a particle. This observation is difficult to rationalize, given the limited end-to-end molecular interactions apparent in Fig. 7 (*top*), especially since there are no Lys residues present in the C-terminal 22 amino acids that could participate in cross-linking. Second, if the parallel model is correct, then none

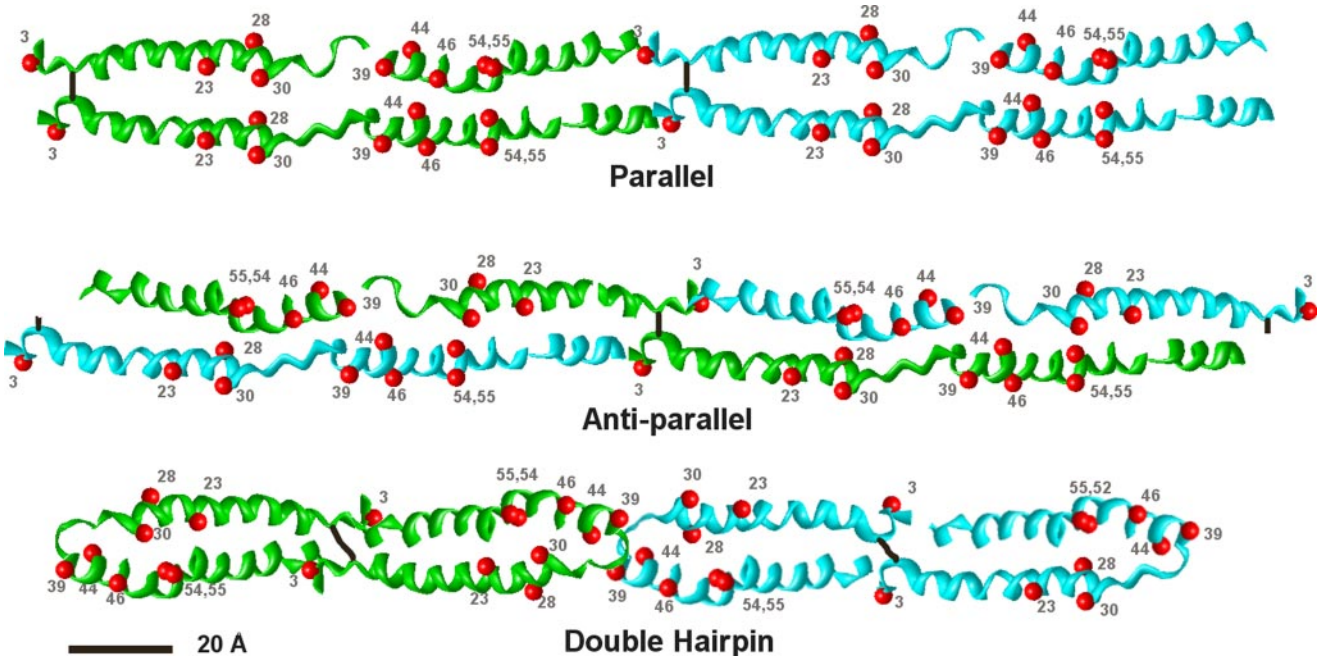

FIGURE 7. **Potential structural models of apoA-II on the edge of a discoidal rHDL particle.** *Top*, parallel model. Two P-Q dimers taken from the crystal structure of apoA-II in association with the detergent BOG are shown (14) as if they had been taken off the edge of a rHDL particle and laid flat on the paper or screen. Only two apoA-II molecules are shown for simplicity (*green* and *blue*), but each particle contains four molecules total. The position of the β-carbon of each Lys residue is shown in *red* and *numbered*. The disulfide bond at Cys[6] of each strand is shown in *black*. *Middle*, antiparallel model. Using the same crystal structure as for the parallel model, one monomer was rotated 180° centered on the disulfide linkage. *Bottom*, double hairpin model. Based on the antiparallel model in the *middle*, the C-terminal 38–40 residues of each strand double back onto the N-terminal half of the strand with an intervening turn sequence. All models are drawn to the same relative scale. The maximum expected length of a BS[3] cross-link (20 Å) is shown by the *black bar*, also drawn to scale.

TABLE 5
Cross-link distance constraint compatibility with the different models in Fig. 7

X-link (Lys-Lys)	Parallel model estimated distance[a]			Antiparallel model estimated distance[b]			Double hairpin model estimated distance[b]		
	Intrastrand (I or II)	Interstrand (III or IV)	Fit?	Intrastrand (I or II)	Interstrand (III or IV)	Fit?	Intrastrand (I or II)	Interstrand (III or IV)	Fit?
	Å			Å			Å		
28–30	5	—[c]	Yes	5	—	Yes	5	—	Yes
30–39	21	—	No	21	—	No	16	—	Yes
39–44	10	—	Yes	10	—	Yes	10	—	Yes
44–46	5	—	Yes	5	—	Yes	5	—	Yes
46–54	12	—	Yes	12	—	Yes	12	—	Yes
28–44	30	33	No	33	20	Yes	18	20	Yes
30–44	27	27	No	27	17	Yes	11	19	Yes
30–46	32	34	No	32	19	Yes	12	26	Yes
30–54	42	45	No	42	12	Yes	7	36	Yes
39–46	12	19	Yes	12	16	Yes	12	16	Yes
39–54	19	29	Yes	19	25	Yes	19	23	Yes
44–54	17	23	Yes	17	31	Yes	17	26	Yes
44–55	15	23	Yes	15	28	Yes	15	25	Yes
46–46	–	12	Yes	—	22	No	—	25	No
Total potential fits[d]			9 of 14			12 of 14			13 of 14

[a] The measurements in Å were taken directly from the P-Q dimer of apoA-II in the BOG crystal structure (14). Since our method could not distinguish between intra- and interstrand cross-links, both possibilities were considered.
[b] The distances measured for the antiparallel and double hairpin models were made graphically at the same scale as the crystal structure and should be considered estimates.
[c] Peptides that were known to be intrapeptide due to their molecular weight were not considered for potential interstrand cross-links.
[d] Potential fits were judged possible if the estimated distance between Lys residues for *either* an intra- or interstrand cross-link fell within 20 Å (sum of the BS[3] spacer arm length of 11.4 Å plus 8.6 Å for two Lys side chains).

of our observed cross-links would be capable of joining two apoA-II molecules together. It is possible that we were unable to detect some cross-links due to poor ionization etc., but given the ease with which apoA-II can be cross-linked on a particle, we find it highly unlikely that we would be unable to detect *any* intermolecular cross-links. In contrast, intermolecular cross-links are extremely plausible in the antiparallel model, in which there are ample opportunities for intermolecular contact. Similarly, the double hairpin model puts clusters of Lys resides in close opposition for forming potential intermolecular cross-links. Third, if the region from 3 to 27 adopts a continuous amphipathic helix, as suggested by some secondary structure prediction algorithms, the Cys residues at position 6 would be predicted to be in the opposite docking interface in the parallel model (Fig. 8) (30). By contrast, in the antiparallel and double hairpin models, the Cys residues would be in an ideal arrangement to form the linkage.

One cross-link that does not strictly fit either the double hairpin or antiparallel models is Lys[46]-Lys[46]. Interestingly, the

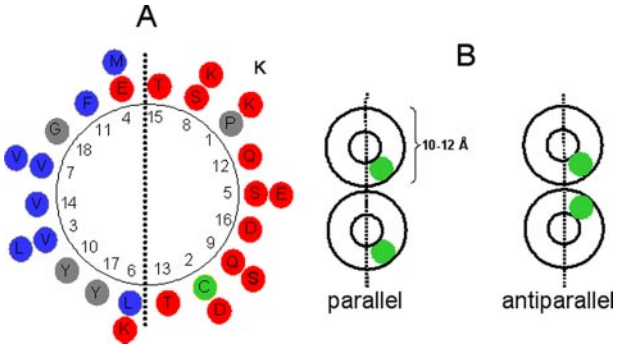

FIGURE 8. **Helical wheel diagram for amino acids 5–21 of apoA-II, indicating potential orientations of Cys[6] for the parallel and antiparallel models.** *A*, the helical wheel for residues 5–21 is shown in *A*, with hydrophobic residues in *blue*, neutral residues in *gray*, and polar residues in *red*. The Cys residues (position 2 in the selected sequence but at position 6 in apoA-II) are shown in *green*. Hydrophobic and hydrophilic phases of the helical wheel are divided by a *dashed line*. *B*, the predicted docking interface for Cys[6] in the parallel and antiparallel models.

crystal structure shows that the region between residues 29 and 39 represents a random coil break in an otherwise helical region. It is possible that this region could be "looped off" of the particle in solution. This would have the effect of bringing residues 29 and 39 much closer together. In this case, it could be envisioned that the Lys[46]-Lys[46] cross-link could be plausible in the anti-parallel model, and slightly more extensive unfolding in this region might make this cross-link plausible in the double hairpin model as well. Indeed, the crystal structure used to generate these models puts apoA-II about 10% more helical than we measured in our CD analysis on particles in solution. One interesting feature of the double hairpin model is that it provides an attractive rationale for the formation of the intrapeptide link between residues 30 and 39. This link is at the limit of the cross-linker range in both the parallel and antiparallel models but is more likely when the hairpin turn puts them into closer opposition. Limited proteolysis of lipidated apoA-II indicated that this region is highly cleavable (15), consistent with a potential turn sequence. Moreover, there is a proline present at position 32, which could be a turn initiator.

In conclusion, our data strongly indicate that apoA-II adopts a beltlike structure in POPC-rHDL particles. Our data are most consistent with the double hairpin model. However, the models proposed in Fig. 7 are based on a crystal structure in which the proteins were under nonnative conditions. There are likely differences in conformation and secondary structure in the truly lipid-bound forms in solution. Thus, the theoretical distances and the putative fits to the data listed in Table 5 should be considered approximations only. Further studies using cross-linking agents that are either not limited to Lys residues or have shorter spacer arm lengths will be required to unambiguously distinguish between the antiparallel and double hairpin models. Nevertheless, this study provides detailed and testable models for lipid-bound apoA-II. This information will be extremely useful for future studies aimed at understanding the structural interactions between apoA-I and apoA-II in more complex forms of HDL. These studies will be critical for evaluating the possibility that apoA-II may function indirectly by modulating apoA-I conformation to affect HDL metabolism *in vivo*.

Acknowledgment—We thank Dr. Timothy A. Keiderling (University of Illinois, Chicago) for generous assistance with CD and fluorescence measurements.

REFERENCES

1. Warden, C. H., Hedrick, C. C., Qiao, J. H., Castellani, L. W., and Lusis, A. J. (1993) *Science* **261,** 469–472
2. Castellani, L. W., Navab, M., Lenten, B. J. V., Hedrick, C. C., Hama, S. Y., Goto, A. M., Fogelman, A. M., and Lusis, A. J. (1997) *J. Clin. Invest.* **100,** 464–474
3. Hedrick, C. C., Castellani, L. W., Wong, H., and Lusis, A. J. (2001) *J. Lipid Res.* **42,** 563–570
4. Escola-Gil, J. C., Marzal-Casacuberta, A., Julve-Gil, J., Ishida, B. Y., Ordonez-Llanos, J., Chan, L., Gonzalez-Sastre, F., and Blanco-Vaca, F. (1998) *J. Lipid Res.* **39,** 457–462
5. Allayee, H., Castellani, L. W., Cantor, R. M., de Bruin, T. W., and Lusis, A. J. (2003) *Circ. Res.* **92,** 1262–1267
6. Bekaert, E. D., Alaupovic, P., Knight-Gibson, C., Norum, R. A., Laux, M. J., and Ayrault-Jarrier, M. (1992) *Biochim. Biophys. Acta* **1126,** 105–113
7. Clay, M. A., Pyle, D. H., Rye, K. A., and Barter, P. J. (2000) *J. Biol. Chem.* **275,** 9019–9025
8. Hime, N. J., Drew, K. J., Wee, K., Barter, P. J., and Rye, K. A. (2006) *J. Lipid Res.* **47,** 115–122
9. Durbin, D. M., and Jonas, A. (1997) *J. Biol. Chem.* **272,** 31333–31339
10. Boucher, J., Ramsamy, T. A., Braschi, S., Sahoo, D., Neville, T. A., and Sparks, D. L. (2004) *J. Lipid Res.* **45,** 849–858
11. Jahangiri, A., Rader, D. J., Marchadier, D., Curtiss, L. K., Bonnet, D. J., and Rye, K. A. (2005) *J. Lipid Res.* **46,** 896–903
12. Davidson, W. S., and RG, D. S. (2005) *Curr. Opin. Lipidol.* **16,** 295–300
13. Gillard, B. K., Chen, Y. S., Gaubatz, J. W., Massey, J. B., and Pownall, H. J. (2005) *Biochemistry* **44,** 471–479
14. Kumar, M. S., Carson, M., Hussain, M. M., and Murthy, H. M. K. (2002) *Biochemistry* **41,** 11681–11691
15. Massey, J. B., Hickson-Bick, D. L., Gotto, A. M., Jr., and Pownall, H. J. (1989) *Biochim. Biophys. Acta* **999,** 121–127
16. Koppaka, V., Silvestro, L., Engler, J. A., Brouillette, C. G., and Axelsen, P. H. (1999) *J. Biol. Chem.* **274,** 14541–14544
17. Schneeweis, L. A., Koppaka, V., Lund-Katz, S., Phillips, M. C., and Axelsen, P. H. (2005) *Biochemistry* **44,** 12525–12534
18. Lund-Katz, S., and Phillips, M. C. (1986) *Biochemistry* **25,** 1562–1568
19. Davidson, W. S., and Hilliard, G. M. (2003) *J. Biol. Chem.* **278,** 27199–27207
20. Silva, R. A., Hilliard, G. M., Li, L., Segrest, J. P., and Davidson, W. S. (2005) *Biochemistry* **44,** 8600–8607
21. Jonas, A. (1986) *Methods Enzymol.* **128,** 553–582
22. Silva, R. A., Hilliard, G. M., Fang, J., Macha, S., and Davidson, W. S. (2005) *Biochemistry* **44,** 2759–2769
23. Sreerama, N., and Woody, R. W. (2000) *Anal. Biochem.* **287,** 252–260
24. Axelsen, P. H., and Citra, M. J. (1996) *Prog. Biophys. Mol. Biol.* **66,** 227–253
25. Maiorano, J. N., Jandacek, R. J., Horace, E. M., and Davidson, W. S. (2004) *Biochemistry* **43,** 11717–11726
26. Panagotopulos, S. E., Horace, E. M., Maiorano, J. N., and Davidson, W. S. (2001) *J. Biol. Chem.* 42965–42970
27. Jonas, A., Wald, J. H., Toohill, K. L., Krul, E. S., and Kezdy, K. E. (1990) *J. Biol. Chem.* **265,** 22123–22129
28. Pliszka, B., Redowicz, M. J., and Stepkowski, D. (2001) *Biochem. Biophys. Res. Commun.* **281,** 924–928
29. Kruip, J., Chitnis, P. R., Lagoutte, B., Rogner, M., and Boekema, E. J. (1997) *J. Biol. Chem.* **272,** 17061–17069
30. De Coen, J. L., Deboeck, M., Delcroix, C., Lontie, J. F., and Malmendier, C. L. (1988) *Proc. Natl. Acad. Sci. U. S. A.* **85,** 5669–5672
31. Sparks, D. L., and Phillips, M. C. (1992) *J. Lipid Res.* **33,** 123–130
32. Koppaka, V. (2001) *Cell. Mol. Life Sci.* **58,** 885–893
33. Markwell, M. A., Haas, S. M., Bieber, L. L., and Tolbert, N. E. (1978) *Anal. Biochem.* **87,** 206–210